of the organic nitrates. In our experiments, all peroxy radicals react with NO. Thus TS1

$$RO_2 + NO \rightarrow RO + NO_2, \tag{1a}$$
$$RO_2 + NO \rightarrow RONO_2. \tag{1b}$$
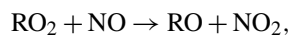
$-d[\beta\text{-ocimene}]/dt = k_2[RO_2][NO]$, where $k_2 = k_{2a} + k_{2b}$, and $d[RONO_2]/dt = k_{2b}[RO_2][NO]$. Thus, $(d[RONO_2]/dt)/(-d[\beta\text{-ocimene}]/dt) = k_{2b}/k_2$. A plot of $\Delta[RONO_2]$ vs. $-\Delta[\beta\text{-ocimene}]$ yields the RO_2-weighted average "branching ratio", k_{2b}/k_2, for the RO_2 radicals produced when OH reacts with β-ocimene in the presence of O_2. We utilized the method of Kwok and Atkinson (1995) to estimate the fraction of time that OH adds to any of carbon no. 1, 2, 3, 4, 6, or 7, with numbers as shown here.
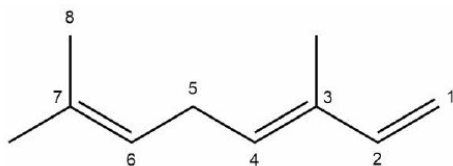
(E)-3,7-dimethylocta-1,3,6-triene

Because of the multiple double bonds at which OH can add, and because of the resonance structures of the multiple allylic radicals produced when OH adds to C no. 1 or 4 (as shown for the most prevalent addition point, C4, in Fig. 2), there are 10 possible main organic nitrate isomers, for each stereoisomer, i.e., the *cis-* or *trans-*β-ocimene, complicating the product analysis. Additional isomers may form from H abstraction from the C5 methylene group, but these are of less significance than the isomers produced from OH addition to the double bond. The measured total hydroxy nitrate, gas-, and particle-phase total organic nitrate yields under different RH conditions are shown in Fig. 3. Yields are corrected for dilution in the chamber, loss to the chamber walls, loss during preconcentration, and hydroxy nitrate consumption by reaction with OH (Rindelaub et al., 2015; Slade et al., 2017). The error bars on individual points reflect the propagated analytical uncertainties of the yields, incorporating all known uncertainties. The analytical uncertainty accounts for analytical errors associated with all the steps involved in sample collection, extraction, and analysis, including denuder and filter extraction and collection efficiencies, uncertainty in the FTIR calibration when using a proxy for -ONO$_2$ quantitation, dilution, wall loss, and consumption by OH. In Fig. 3, we see that the observed total RONO$_2$ yield and that for both gas and aerosol phases, and for the CIMS-determined hydroxy nitrates, are RH dependent, decreasing by $\sim \times 2$ over the range studied ($\sim$ 3–70 % RH). The decrease indicates that hydroxy nitrates partition to the aerosol phase, where they are lost by hydrolysis, which was previously observed in the case of α-pinene (Rindelaub et al., 2015). At higher RH, there will be more water associated with the particles, and the hydroxy nitrates are then more particle soluble (Rindelaub et al., 2015). If we then extrap-

olate to 0 % RH, the extent of particle-phase loss will be minimized, and thus the intercept represents the determined lower limit to the yield, assumed to represent the fraction of peroxy radicals reacting with NO that react to produce RONO$_2$. The intercept for the total RONO$_2$ yield, as shown in Fig. 3, is 38($\pm$9) %, represented by the y intercept of the black symbols in Fig. 3a. In Fig. 4, we present a summary of a range of previous observations of branching ratios for alkanes, alkenes, isoprene, and the two terpenes for which we have determined the total yield (assumed RO$_2$-weighted average branching ratio). It is shown that the branching ratio for β-ocimene- and α-pinene-derived RONO$_2$ follows the trend observed for simple alkanes, within the uncertainty of the measurements (Arey et al., 2001; Rindelaub et al., 2015; Teng et al., 2015, 2017; Xiong et al., 2015).

We found that the first-generation hydroxy nitrates exist primarily in the gas phase (red markers in Fig. 3a), which is consistent with the low SOA yield, shown in Fig. 5. Although the total RONO$_2$ yield of β-ocimene is greater than that for α-pinene oxidation, the particle-phase organic nitrate yield is much larger in the α-pinene case (Rindelaub et al., 2015). This is likely due to the fact that the SOA yield is much larger for α-pinene (34 $\pm$ 12 %; Rindelaub et al., 2016a), since, as discussed in the next section, β-ocimene oxidation produces smaller, more volatile acyclic oxidation products. However, some of the low particle-phase RONO$_2$ yield must occur because of the hydrolysis in the aerosol phase. The relatively low SOA yield for β-ocimene can be attributed to the alkoxy radical decomposition products that produce the remaining 62 % of the first-generation oxidation products following the OH-initiated pathway in the presence of NO$_x$, for example as shown producing methyl vinyl ketone and 2-methyl-2-pentenal in Fig. 2. These decomposition products are expected to be primarily C6 and smaller carbonyl compounds, of much greater volatility than the β-ocimene hydroxy nitrate. This occurs in the case of this linear tri-alkene, because scission of the C–C bond at the α position to the alkoxy radical breaks the carbon chain into smaller chain carbonyl compound products, as shown in Fig. 2. As previously stated, the expected first-generation oxidation products (Fig. 2) are in the upper range of semi-volatile species, confirming their preferential presence in the gas phase (Donahue et al., 2011).

The CIMS-measured hydroxy nitrate yields (green markers in Fig. 3a) are lower than the total gas-phase RONO$_2$ yield (from FTIR), likely due to a lower CIMS sensitivity to the β-ocimene hydroxy nitrates than assumed, using the α-pinene hydroxy nitrate standard as a proxy. However, it is important to note that we expect all organic nitrates in this system to be hydroxy nitrates. In this regard, it is important that the CIMS-observed hydroxy nitrate concentration decayed to the same relative extent as for the FTIR-determined total, as shown in Fig. 3. When the hydroxy nitrate undergoes hydrolysis, the reaction proceeds likely via SN1 unimolecular nucleophilic substitution, as discussed in Rindelaub et al. (2015). The nitrooxy functional group serves as